YGR042W/MTE1 Functions in Double-Strand Break Repair with *MPH1*

Askar Yimit*, TaeHyung Kim†, Ranjith P. Anand‡, Sarah Meister*, Jiongwen Ou*, James E. Haber‡, Zhaolei Zhang† and Grant W. Brown*,1

*Department of Biochemistry and Donnelly Centre, University of Toronto, Toronto, Ontario, Canada, †Department of Computer Science and Donnelly Centre, University of Toronto, Toronto, Ontario, Canada, ‡Rosenstiel Basic Medical Sciences Research Center, Brandeis University, Waltham, Massachusetts

ABSTRACT Double-strand DNA breaks occur upon exposure of cells to agents such as ionizing radiation and ultraviolet light or indirectly through replication fork collapse at DNA damage sites. If left unrepaired double-strand breaks can cause genome instability and cell death. In response to DNA damage, proteins involved in double-strand break repair by homologous recombination re-localize into discrete nuclear foci. We identified 29 proteins that co-localize with the recombination repair protein Rad52 in response to DNA damage. Of particular interest, Ygr042w/Mte1, a protein of unknown function, showed robust colocalization with Rad52. Mte1 foci fail to form when the DNA helicase Mph1 is absent. Mte1 and Mph1 form a complex, and are recruited to double-strand breaks *in vivo* in a mutually dependent manner. Mte1 is important for resolution of Rad52 foci during double-strand break repair, and for suppressing break-induced replication. Together our data indicate that Mte1 functions with Mph1 in double-strand break repair.

KEYWORDS DNA repair; recombination; double strand breaks; break-induced replication; loss of heterozygosity; nuclear foci

Effective repair of double-strand DNA breaks (DSBs) is critical to the preservation of genome stability, yet most modes of DSB repair have significant potential to generate sequence alterations or sequence loss. Repair of DSBs by homologous recombination can result in loss of heterozygosity when resolution of recombination intermediates between homologous chromosomes results in a crossover. As such, cells possess several mechanisms by which crossing over can be suppressed in favor of non-crossover recombination products. Double Holliday junction intermediates that result from invasion of a homologous chromosome by both ends of a resected DSB (Szostak *et al.* 1983) can be resolved nucleolytically, by the action of the Yen1 and Mus81/Mms4 endonucleases (Blanco *et al.* 2010; Ho *et al.* 2010), to produce a random distribution of crossover and non-crossover products. By contrast, the same dHJ intermediates can be dissolved by the combined helicase and ssDNA decatenase action of the BTR complex (Sgs1/Top3/Rmi1 in yeast) (Wu *et al.* 2006; Yang *et al.* 2010) to yield exclusively non-crossover products (Wu and Hickson 2003). Crossovers can also be prevented if the D-loop structure that results from the first strand invasion by one end of a resected DSB into the homologous chromosome is unwound before capture of the second end to form the dHJ. Unwinding of D-loops is catalyzed *in vitro* and *in vivo* by the 3′ to 5′ DNA helicase Mph1 (Prakash *et al.* 2009; Sun *et al.* 2008) in order to prevent loss of heterozygosity due to crossovers and break-induced replication (Luke-Glaser and Luke 2012; Mazon and Symington 2013; Stafa *et al.* 2014).

The Mph1 DNA helicase was first identified as a deletion mutant with an increased mutation frequency (Entian *et al.* 1999). Subsequent characterization revealed that *mph1* mutants are sensitive to the alkylating agent MMS, and to a lesser degree to ionizing radiation (Scheller *et al.* 2000), and that *mph1* mutants are proficient for mitotic recombination (Schurer *et al.* 2004). Molecular insight into Mph1 function in recombination reactions comes from evidence that Mph1 is a DNA helicase (Prakash *et al.* 2005), and that Mph1 can unwind Rad51 D-loops (Prakash *et al.* 2009; Sun *et al.* 2008) and extended D-loops (Sebesta *et al.* 2011). Consistent with an anti-recombination role for Mph1, overexpression of *MPH1* reduces recombination rate and reduces loading of Rad51 at an induced DSB (Banerjee *et al.* 2008). Indeed, Mph1 suppresses crossing over during mitotic recombination, likely by unwinding D-loop recombination intermediates formed by Rad51 (Prakash *et al.* 2009) and preventing ectopic resolution of early strand exchange intermediates by the Mus81-Mms4 nuclease (Mazon and Symington 2013). Mph1 inhibits break-induced replication (BIR) repair of double-strand breaks (Luke-Glaser and Luke 2012) and promotes template switching during BIR (Stafa *et al.* 2014), both consistent with the ability of Mph1 to unwind recombination intermediates *in vitro*. In addition to functioning in crossover suppression, Mph1 plays a pro-recombinogenic role in repair of stressed DNA replication

Manuscript compiled: Sunday 22nd November, 2015
[1]Department of Biochemistry, University of Toronto, Donnelly Centre, Room 1206, 160 College Street, Toronto, Ontario M5S 3E1, Canada Tel.: +1 416 946 5733; Fax: +1 416 978 8548 E-mail: grant.brown@utoronto.ca

forks (Chavez *et al.* 2011; Chen *et al.* 2009 2013; Choi *et al.* 2010; Sun *et al.* 2008; Xue *et al.* 2014; Zheng *et al.* 2011), and inhibits non-homologous end-joining repair at telomeres (Luke-Glaser and Luke 2012). Mph1 is thought to be the functional homologue of the human FANCM protein. Thus, available evidence points to diverse functions for Mph1, and these functions are likely connected to the ability of Mph1 to unwind and remodel DNA structures.

Here we leverage intracellular protein location data to identify the complement of proteins that co-localize with the recombination repair protein Rad52 in nuclear foci during the response to DNA double-strand breaks. In addition to defining the membership of Rad52 foci, we identify an uncharacterized protein, Ygr042w/Mte1, that functions in double-strand break repair. Mte1 acts in complex with Mph1 at double-strand breaks *in vivo*, is important for DSB repair as assessed by resolution of Rad52 foci, and functions, as is the case for Mph1, in suppressing break-induced replication repair of double-strand DNA breaks.

Materials and Methods

Yeast strains and media

All yeast strains used in this study are derivatives of BY4741 (Brachmann *et al.* 1998), CL11-7, or W303, and are listed in Table S1. Strains were constructed using genetic crosses and standard PCR-based gene disruption techniques. Standard yeast media and growth conditions were used.

Chromatin immunoprecipitation and deep sequencing

Chromatin immunoprecipitation was performed using Flag-epitope tagged versions of each indicated protein, as previously described (Balint *et al.* 2015; Roberts *et al.* 2008), with modifications. Cells were grown to mid-logarithmic phase in YPR (1% yeast extract, 2% peptone, 3% raffinose) at 28°C and then arrested in G2/M with 20 μg/ml nocodazole for 4 hrs. Galactose was added to 2% final to induce expression of the HO endonuclease. Cells were sampled before galactose addition and after 4 hours of induction, and cross-linked with formaldehyde overnight. Cells were harvested and washed twice with cold TBS (20 mM Tris-HCl pH 7.5, 150 mM NaCl), resuspended in FA-lysis buffer (50 mM HEPES pH 7.5, 2 mM EDTA, 1% Triton X-100, 0.1% sodium deoxycholate, 150 mM NaCl) containing 0.05% SDS, lysed and sonicated. Immunoprecipitates were washed sequentially with 1 ml of FA-lysis buffer, FA-lysis buffer containing 1M NaCl, FA-lysis buffer containing 0.5M NaCl, Wash Buffer (50 mM HEPES pH 7.5, 0.25M LiCl, 2 mM EDTA, 1% Triton X-100, 1% sodium deoxycholate, 1% NP-40, 10 mM Tris-HCl pH 8.0), and TE (10 mM Tris-HCl pH 8.0, 1 mM EDTA). Protein-DNA complexes were eluted, cross-links were reversed, protein and RNA was digested, and DNA was isolated by phenol/chloroform extraction and ethanol precipitation. Sequencing libraries were generated using the Nextera XT DNA Sample Preparation Kit (Illumina) with custom index primers for the PCR amplification step. Libraries were quantified using a 2100 Bioanalyzer (Agilent) and the KAPA SYBR FAST Universal qPCR Kit (KAPA Biosystems).

Sequencing data analysis

Input and IP samples from each experiment were sequenced on an Illumina HiSeq 2500 (50 nucleotide single-end reads). All sequencing data are deposited in the Sequence Read Archive (http://www.ncbi.nlm.nih.gov/sra, study accession SRP064493). The number of reads for each sample ranges from 12.8 M – 25.7 M. The quality of sequencing reads was first assessed using FastQC. (http://www.bioinformatics.bbsrc.ac.uk/projects/fastqc). All samples have a median PHRED score of 30 or higher for all positions. Sequenced reads were mapped to the *S. cerevisiae* reference genome version WS220 (downloaded from the Saccharomyces Genome Database (Cherry *et al.* 2012; Engel *et al.* 2014)) using Bowtie2 (version 2.0.0) (Langmead and Salzberg 2012) with default settings, except for forcing end-to-end alignment. Greater than 96% mapping rates were achieved for all samples, yielding a minimum 50x coverage for all samples (Table S2). In order to reduce any bias from DNA sequencing, the data were normalized by the ratio of coverage for each IP and input pair prior to each comparison. We used a 100 bp sliding window with a step size of 50 bp to calculate enrichment scores as a log2 ratio of normalized read counts for each IP:input pair. For the enrichment scores displayed in Figure 5, the enrichment score for each of the 0h samples was subtracted from each of the matched 4h samples. Figure S1 displays the enrichment scores for all of the IP:input pairs.

Whole cell extracts, immunoblotting and immunoprecipitation

Logarithmically growing cells at 30°C were treated with or without 5 μg/ml phleomycin (BioShop PEO422.25) for 2 hours before cells were collected, fixed with 10% trichloroacetic acid, and whole cell extracts were prepared (Pellicioli *et al.* 1999). Proteins were resolved by SDS-PAGE and subjected to immunoblotting with α-Flag M2 (F3165, Sigma-Aldrich), α-HA (ab16918, Abcam), or α-tubulin (YOL1/34, Serotec) antibodies. Native extracts for immunoprecipitation were prepared from $5x10^8$ cells as previously described (Shimomura *et al.* 1998), with some modifications. Cell pellets were resuspended in FA-lysis buffer containing 1 mM DTT, 2 mM sodium fluoride, 1 mM sodium ortho-vanadate, 1X Complete Mini EDTA-free protease inhibitor cocktail (Roche 11836170001), 2.5 μg/ml aprotinin, 10 mM β-glycerophosphate, 5 μg/mL leupeptin, 2 μg/mL pepstatin A, 1 mM PMSF, and 5 μg/ml TLCK, then lysed with glass beads. Cleared extracts were immunoprecipitated with α-Flag M2 antibody. Beads were washed twice with 0.5 ml FA-lysis buffer as above, and eluted in 5X SDS loading buffer.

DNA damage sensitivity

Yeast strains were grown overnight in YPD, diluted serially, and spotted onto YPD plates containing the indicated concentrations of phleomycin. Plates were incubated at 30°C for 2-3 days before imaging.

Fluorescence microscopy

For analysis of GFP fusion protein nuclear foci, strains were grown to mid-log phase in YPD, diluted into fresh YPD and cultured overnight to OD_{600} = 0.3. Cells were treated for 120 minutes with 5 μg/ml phleomycin, or cultured without phleomycin, harvested, and washed once in low fluorescence medium with or without phleomycin before imaging. Eleven z slices with a 0.4 μm step size were acquired using Volocity imaging software (PerkinElmer) controlling a Leica DMI6000 confocal fluorescence microscope with fluorescein isothiocyanate, Texas Red and differential interference contrast filter sets (Quorum Technologies). Images were scored by visual inspection for GFP fusion protein foci. Samples were compared using the t-test or the Wilcoxon rank sum test, as appropriate, in R (www.r-project.org). Data

were plotted using ggplot2, in R. For Rad52-GFP foci, the same procedure was used except that cells were blocked in G2/M phase by treatment with 20 μg/ml nocodazole for 3 hours, and exposed to 50 μg/ml phleomycin for 30 minutes.

Recombination assays

Recombination rates were calculated using a direct repeat recombination assay (Smith and Rothstein 1999) and quantifying recombination from the number of Leu+ recombinant colonies using the method of the median (Lea and Coulson 1949). Each fluctuation test comprised 9 independent cultures, and the results from 10 fluctuation tests were plotted in R. Rates were compared using a Welch two-sample t-test in R.

BIR efficiencies were calculated as described previously (Anand *et al.* 2014). Briefly, cells were plated for individual colonies on YEPD + clonNat to retain the HOcs (which is marked with *natMX*). Approximately one million cells from individual colonies were appropriately diluted and plated on YEPD plates to get the total cell count and on YEP-Gal plates for HO induction. Cells that grew on YEP-Gal plates (DNA break-survivors) were counted and replica plated to plates lacking uracil to determine BIR frequencies. For each replicate, Ura+ frequencies were calculated as the total Ura+ cells that grew on plates lacking uracil over the total cells on YEPD. Experiments were repeated at least 3 times, plotted in R, and compared using a Welch two-sample t-test in R.

Data Availability

Strains are available upon request. Table S1 contains the genotypes of all strains used. Table S2 contains statistics for all deep sequencing, including NCBI Sequence Read Archive (SRA) accession numbers.

Results

Twenty-nine proteins form nuclear foci that detectably co-localize with Rad52 foci

A number of DNA repair proteins change their intracellular localization from pan-nuclear to nuclear foci in response to DNA damage. Proteins that localize in nuclear foci have been identified in candidate approaches (Burgess *et al.* 2009; Germann *et al.* 2011; Lisby *et al.* 2004 2001; Melo *et al.* 2001; Zhu *et al.* 2008) and in genome-scale screens (Denervaud *et al.* 2013; Mazumder *et al.* 2013; Tkach *et al.* 2012; Yu *et al.* 2013). Nuclear foci are commonly thought of as centers of DNA repair, in part because foci formed by recombination repair proteins co-localize with double-strand

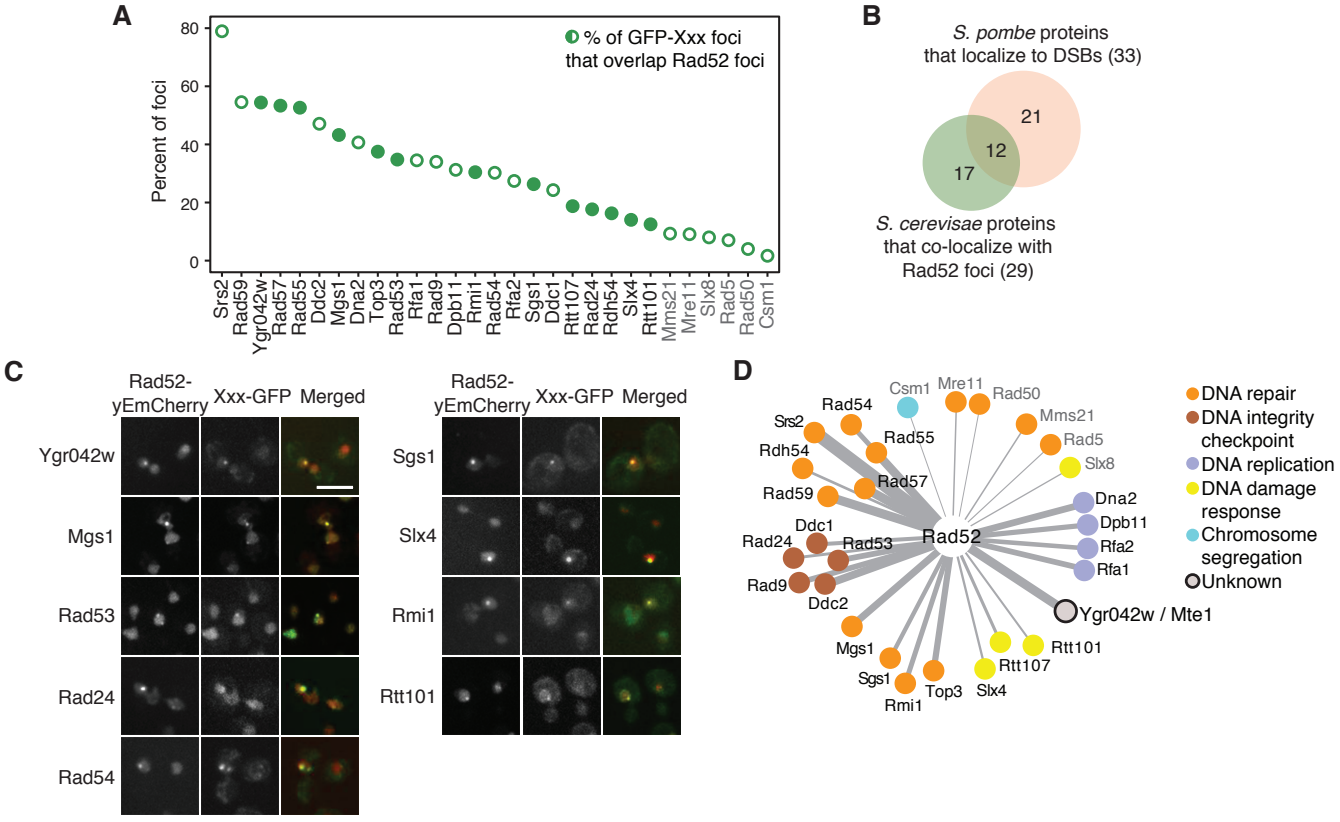

Figure 1 Twenty-nine proteins form nuclear foci that detectably co-localize with Rad52 foci. (A) The percent of nuclear foci formed by each GFP fusion protein that overlap with Rad52-yEmCherry foci after 2 hours in 5 μg/ml phleomycin is plotted. Open circles indicate co-localizations that were previously identified. Closed circles indicate Rad52 co-localizations that have not been previously described. Protein names in grey indicate those with a percent co-localization at or below that seen with Mre11. (B) The overlap between the proteins that co-localize with Rad52 foci and those that co-localize with an induced double-strand DNA break in fission yeast is shown. (C) Representative fluorescence micrographs showing co-localization of the indicated GFP fusion proteins with Rad52 foci. The mCherry, GFP, and merged images are shown. The scale bar is 5 μm. (D) A network of the proteins that co-localize detectably with Rad52. Protein function is indicated by colour and edge thickness is proportional to the extent of protein co-localization with Rad52 foci.

DNA breaks (Lisby *et al.* 2003). However, not all nuclear foci are identical to the canonical DNA repair centers that are marked by the recombination protein Rad52. For example, Cmr1 forms foci that do not co-localize detectably with Rad52 (Tkach *et al.* 2012), but rather co-localize with a distinct set of proteins in an intranuclear quality control compartment (Gallina *et al.* 2015).

We tested 61 budding yeast proteins that form nuclear foci in response to DNA damage to identify those that co-localize detectably with Rad52. Nuclear foci proteins were tagged with GFP (Huh *et al.* 2003), Rad52 was tagged with mCherry, and cells were examined by fluorescence microscopy after treatment with the double-strand DNA break inducing agent phleomycin (Figure 1). Twenty-nine proteins co-localized detectably with Rad52 (Figure 1A and Tables S3, S4, and S5). The extent of co-localization ranged from 79% of foci for Srs2, to 2% of foci for Csm1 (Table S3). Fourteen proteins had not previously been described as components of Rad52 foci (Figure 1A and 1C), although most are known DNA repair, DNA replication, or checkpoint signaling proteins (Figure 1D). We identified one protein, Ygr042w, with no known role in recombination repair. Mutants in *YGR042W* affect telomere length (Askree *et al.* 2004), and the fission yeast homologue of Ygr042w, Dbl2, forms foci that co-localize with an induced double-strand DNA break (Yu *et al.* 2013). The extensive co-localization of Ygr042w with Rad52 foci, similar to the extent of co-localization observed for members of the Rad52 epistasis group (Symington 2002) Rad55, Rad57, and Rad59, suggests that Ygr042w could function in repair of double-strand DNA breaks. While this work was in progress, a name for *YGR042W* was reserved in the Saccharomyces Genome Database, *MTE1* (Mph1-associated Telomere maintenance protein). Thus, we now refer to *YGR042W* as *MTE1*.

Mte1 foci form in S/G2 phase and in response to double-strand breaks

The foci formed by Mte1 in response to phleomycin localize to the nucleus (Figure 2A) and form more frequently in cells in S and G2 phases than in G1 cells (Figure 2B). Mte1 foci also form in the absence of DNA damaging agents, in 13% of cells during S or G2 phase, but in only 3% of cells during G1 phase (Figure 2B), similar to Rad52 foci (Lisby *et al.* 2001). As expected, Mte1 foci levels increase with increasing phleomycin concentration and with increasing time of phleomycin exposure (Figure 2C). Deletion of *MTE1* confers modest sensitivity to phleomycin, but not to other DNA damaging and replication stress agents, methyl methanesulfonate, hydroxyurea, and camptothecin (Figure 2D).

Mte1 foci are increased when end-resection is defective and depend on MPH1

We tested whether Mte1 focus formation was altered in mutants of genes encoding other nuclear focus proteins and several additional DNA repair proteins. Of the 52 mutants tested, 5 led to increased Mte1 focus formation (Figure 3A and Table S6). Three of the mutants, in *MRE11*, *RAD50*, and *XRS2*, would eliminate the DSB end-resection function of the MRX complex (Ivanov *et al.* 1994), and *RAD52* is critical for formation of the Rad51 filament at resected DSBs (Sugawara *et al.* 2003), among other functions. Mte1 foci increase in both the presence and absence of phleomycin in *mre11*Δ, *rad50*Δ, *xrs2*Δ, and *rad52*Δ, indicating that spontaneous DSBs are either more prevalent in these mutants, or are repaired less effectively. By contrast, the *rad9*Δ mutant, which is defective in DNA damage checkpoint signaling and results in faster end-resection at a double-strand break (Ferrari *et al.* 2015; Lazzaro *et al.* 2008), displays increased Mte1 foci only in the presence of phleomycin. We tested whether other checkpoint mutants result in increased Mte1 foci (Figure 3A). We disrupted checkpoint signaling upstream of Rad9, by deleting *MEC1*, *TEL1*, or both, and found that only the *mec1*Δ *tel1*Δ double mutant had a statistically evident increase in Mte1 foci, in both the absence and presence of phleomycin ($p=5.2\times10^{-5}$ and p=0.00095, one-sided t-test). Interestingly, *mec1*Δ *tel1*Δ cells, like *rad9*Δ, have a higher rate of resection (Tsabar *et al.* 2015), and so increased Mte1 foci in these mutants could reflect increased resection of the DSB.

Two mutants, *mph1*Δ and *rpa2-ph*, caused decreased Mte1 focus formation (Figure 3B). Mph1 and RPA are proposed to function together to suppress recombination (Banerjee *et al.* 2008).

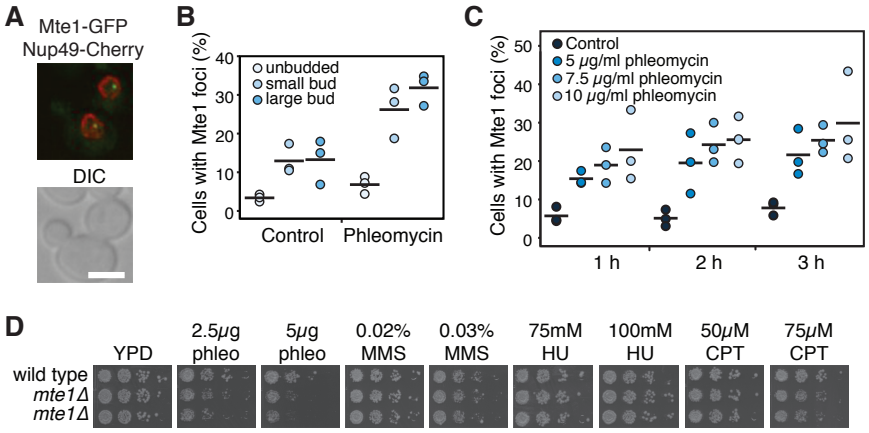

Figure 2 Mte1 foci form in S/G2 phase and in response to double strand breaks. (A) Mte1-GFP nuclear foci are shown in a merged fluorescence micrograph. The lower panel is the DIC image of the same cells. The scale bar is 5 μm. (B) The fraction of unbudded, small-budded, and large-budded cells with Mte1 nuclear foci after 2 hours in 5 μg/ml phleomycin is plotted. The black bars show the means of the 3 replicates. (C) The fraction of cells with Mte1 nuclear foci after 1, 2, or 3 hours in the indicated concentrations of phleomycin is plotted. The black bars show the means of the 3 replicates. (D) Serial ten-fold dilutions of the indicated strains were spotted on the indicated concentrations of phleomycin (phleo), methyl methanesulfonate (MMS), hudroxyurea (HU), or camptothecan (CPT). Plates were photographed after 2 to 3 days.

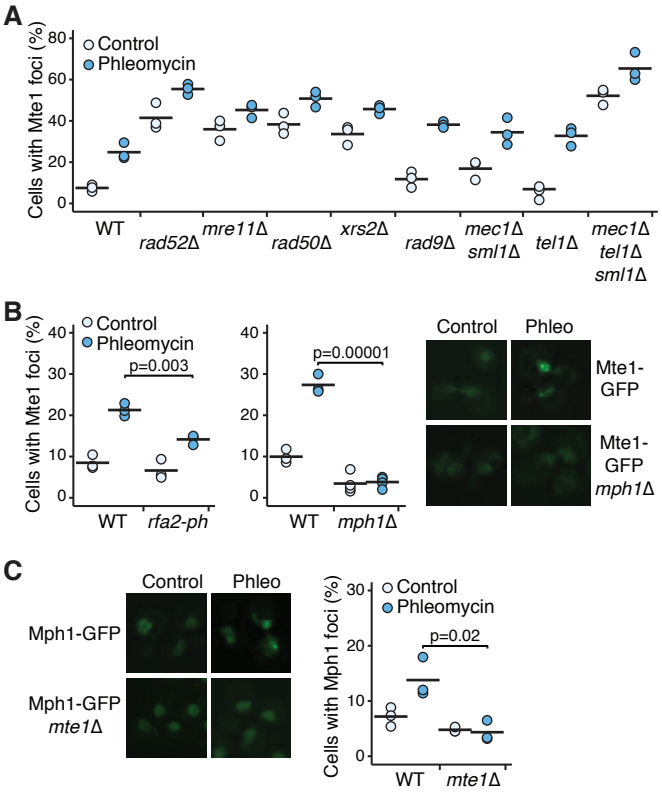

Figure 3 Mte1 foci are increased in *MRX* mutants and depend on *MPH1*. (A) The percent of cells with Mte1 foci is plotted for mutants with increased numbers of foci. Three replicates for each strain, in the absence and presence of 5 μg/ml phleomycin, are plotted. The black bars show the means of the 3 replicates. N ranged from 41 to 211 cells per strain per replicate. (B) The percent of cells with Mte1 foci is plotted for mutants with decreased numbers of foci (left), for untreated cells and cells grown in the presence of 5 μg/ml phleomycin for 2 hours. The black bars show the means of the replicates. The indicated samples were compared using a one-sided t-test. N ranged from 65 to 174 cells per strain per replicate. Representative images (right) of cells with Mte1 foci are shown for untreated cells and cells grown in the presence of 5 μg/ml phleomycin for 2 hours, for wild type cells and *mph1*Δ cells. (C) Representative images (left) and the percent of cells with Mph1 foci (right) are shown for untreated cells, and cells grown in the presence of 5 μg/ml phleomycin for 2 hours, for wild type cells and *mte1*Δ cells. The black bars show the means of the replicates. The indicated samples were compared using a one-sided t-test. N ranged from 89 to 276 cells per strain per replicate.

Mph1 forms nuclear foci in unperturbed cells and in MMS (Chen *et al.* 2009), and we find that Mph1 foci increase in the presence of phleomycin (Figure 3C). Deletion of *MTE1* reduces Mph1 foci to background levels (Figure 3C), suggesting that Mph1 and Mte1 might function in concert.

Mte1 and Mph1 interact physically and are in the same genetic pathway

We tested whether Mte1 interacts with Mph1 in co-immunoprecipitation experiments (Figure 4). We found that Mte1 immunoprecipitates contain Mph1 (Figure 4A) and that Mph1 immunoprecipitates contain Mte1 (Figure 4B). Mte1 and Mph1 appear to interact constitutively, as the extent of co-immunoprecipitation is unaffected by the presence of phleomycin. Consistent with Mte1 and Mph1 forming a complex, 38% of Mte1 foci co-localize with Mph1 after 3h in phleomycin (Figure 4C). Both *mte1*Δ and *mph1*Δ confer modest sensitivity to phleomycin, and the double mutant *mte1*Δ *mph1*Δ is no more sensitive than either of the single mutants, suggesting the *MTE1* and *MPH1* function in the same genetic DSB response pathway. By contrast, *mte1*Δ and *rad52*Δ show additive phleomycin sensitivity (Figure 4D and 4E) suggesting that *MTE1* and *RAD52* play non-redundant roles in DSB repair.

Mte1 and Mph1 localize to double-strand DNA breaks

Many proteins involved in double-strand DNA break repair are physically associated with chromatin adjacent to strand breaks *in vivo*, including Mph1 (Prakash *et al.* 2009). We used chromatin immunoprecipitation followed by deep sequencing to assess the binding of Mte1 and Mph1 to the region flanking an induced HO double-strand break (Figure 5). The HO double-strand break was induced by growth in galactose to induce expression of the HO endonuclease. Cultures were sampled before HO induction, and after 4 hours in galactose, cross-linked with formaldehyde, and subjected to chromatin immunoprecipitation. The enrichment of DNA sequences in the immunoprecipitate relative to the input sample indicates regions of protein binding. We first tested Rad52, which is known to localize robustly to DSBs *in vivo* (Wolner *et al.* 2003), and found a peak of enrichment on chromosome III following HO induction, centered on the HO endonuclease site, (Figure 5A and Figure S1). Similar peaks were detected at the induced DSB for both Mte1 and Mph1, indicating that the Mte1-Mph1 protein complex is recruited to DNA double-strand breaks *in vivo* (Figure 5A and S1). Of particular interest, the Mte1 enrichment at the DSB was reduced in an *mph1*Δ mutant, and Mph1 enrichment at the DSB was reduced in an *mte1*Δ mutant (Figure 5A and S1). Mte1 and Mph1 protein levels were unchanged in the mutant backgrounds (Figure 5B), suggesting that the functional unit recruited to DSBs is an Mte1-Mph1 complex.

Increased phleomycin-induced DSBs in the absence of Mte1

The presence of Mte1 at an induced DSB, and the sensitivity of *mte1*Δ strains to DSBs, suggested that Mte1 could play a role in DSB repair. We measured Rad52 focus formation as a proxy for the presence of DNA damage. Cells were blocked in G2 phase with nocodazole and treated with 50 μg/ml phleomycin for 30 minutes. Phleomycin caused an increase in the fraction of cells with Rad52 foci in *mph1*Δ, *mte1*Δ, and the *mph1*Δ *mte1*Δ double mutant compared to the wild-type (Figure 6A), and an increase in Rad52 focus intensity (Figure 6B). The *mph1*Δ and *mte1*Δ single mutants and the *mph1*Δ *mte1*Δ double mutant had similar effects in both assays, suggesting that Mte1 and Mph1 function together in DSB repair. We measured recombination directly in *mte1*Δ mutants (Figure 6C). In the absence of DNA damage, *mte1*Δ, like *mph1*Δ (Schurer *et al.* 2004), is proficient in mitotic recombination, displaying a recombination rate that is highly similar to the wild type.

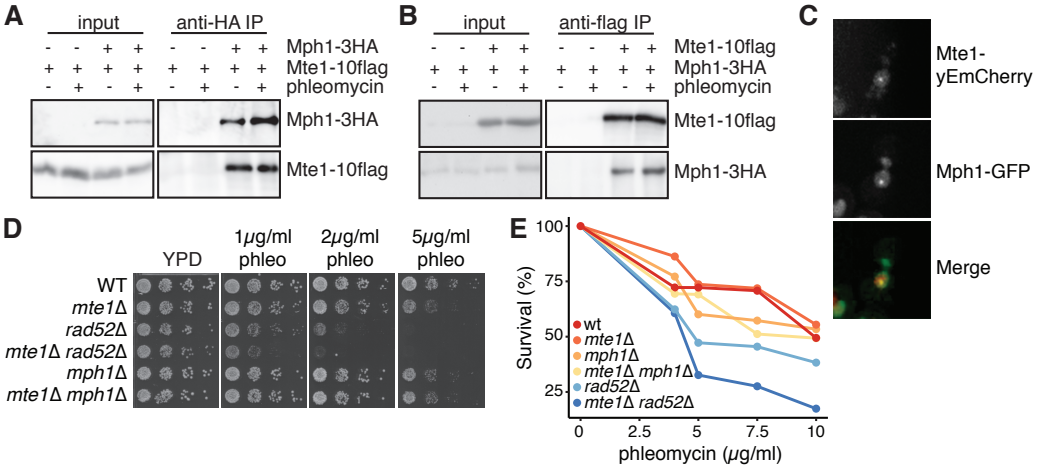

Figure 4 Mte1 and Mph1 interact physically and are in the same genetic pathway. (A) Extracts of cells expressing Mte1-10flag and Mph1-3HA proteins as indicated were subjected to immunoprecipitation with an anti-HA antibody. Input and immunoprecipitate (IP) fractions were immunoblotted to detect Mte1-10flag or Mph1-3HA. (B) In the reciprocal of panel A, extracts of cells expressing Mte1-10flag and Mph1-3HA proteins as indicated were subjected to immunoprecipitation with an anti-flag antibody. Input and immunoprecipitate (IP) fractions were immunoblotted to detect Mte1-10flag or Mph1-3HA. (C) Representative fluorescence micrographs showing co-localization of Mte1 with Mph1 following phleomycin treatment. The mCherry, GFP, and merged images are shown. (D) Serial ten-fold dilutions of the indicated strains were spotted on media containing the indicated concentrations of phleomycin. Plates were photographed after 2 to 3 days. (E) The indicated strains were cultured in the presence of the indicated concentrations of phleomycin for 2 hours, diluted and plated on media lacking phleomycin. The fraction of cells that formed colonies is plotted.

Mte1 suppresses break-induced replication

Mph1 suppresses break-induced replication during double-strand break repair (Luke-Glaser and Luke 2012; Stafa *et al.* 2014). Given the physical and genetic interactions between Mte1 and Mph1 that our work has revealed, we tested whether Mte1 also plays a role in suppressing BIR. We induced a DSB in strains carrying a modified chromosome V with a truncated *ura3* allele adjacent to an HO endonuclease site. Upon induction of the double-strand break, the truncated allele is repaired using donor sequences located on the other arm of chromosome V to yield Ura+ colonies (Figure 6D). In homologous BIR, where the sequences that recombine share 108 bp of homology, deletion of *mte1* results in increased BIR (Figure 6E), similar to deletion of *mph1* (Stafa *et al.* 2014). Thus, Mte1, like Mph1 is an important suppressor of break-induced replication and therefore a suppressor of loss of heterozygosity.

Discussion

In response to DNA damage, most homologous recombination proteins are recruited to the sites of double-strand DNA breaks. Among them, Rad52 is a key recombination protein and the Rad52 focus is considered to be a sensitive indicator of DNA repair (Alvaro *et al.* 2007; Lisby *et al.* 2003 2001). We identified 29 proteins that localize to Rad52 foci in response to DNA damage. Among them, we identified a role for *YGR042W/MTE1* in DNA double-strand break repair. Similar to many DNA repair proteins, Mte1 forms nuclear foci in response to double-strand breaks and Mte1 foci only form when the DNA helicase Mph1 is present. Mte1 forms protein complexes with Mph1, and both proteins are recruited to the chromatin flanking double-strand DNA breaks *in vivo*. In the absence of Mte1 the Rad52 repair centers accumulate, and Mte1 is important for suppressing break-induced replication. Together our data indicate that the function of Mph1 in recombination repair of double-strand breaks requires Mte1.

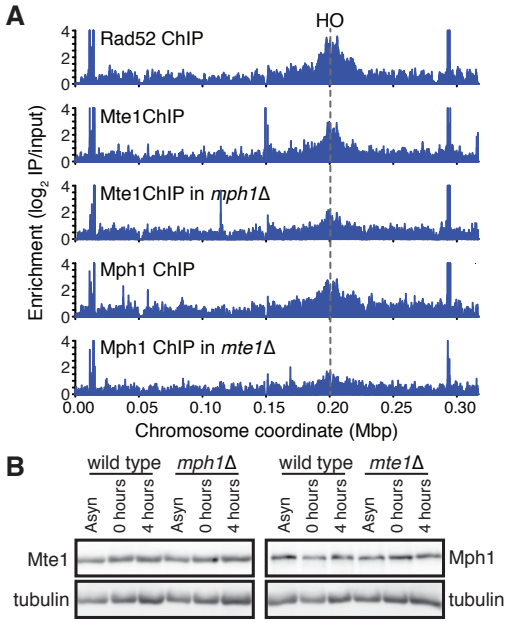

Figure 5 Mte1 and Mph1 are recruited to double-strand DNA breaks. (A) ChIP-seq analysis was performed on *RAD52-FLAG*, *MTE1-FLAG*, *MTE1-FLAG mph1*Δ, *MPH1-FLAG*, and *MPH1-FLAG mte1*Δ cells at 0h and 4h following the induction of a specific double-strand break at the *MAT* locus by the HO endonuclease. ChIP enrichment scores derived by subtracting the log2 immunoprecipitate to input ratio at 0h from the ratio at 4h are plotted across chromosome III. The position of the HO cut site is indicated. (B) Extracts from cells used in panel A were subjected to immunoblot analysis, and probed with an anti-flag antibody and an anti-tubulin antibody (as a loading control).

How does Mte1 impact Mph1 function?

Mte1 and Mph1 appear to be members of a constitutive complex. The interaction between the two proteins, whether direct or indirect, was readily detected by co-immunoprecipitation of either protein even in the absence of DNA damage. Mte1 is important for Mph1 nuclear focus formation, and more importantly, for the recruitment of Mph1 to double-strand breaks *in vivo*. These data suggest that Mph1 functions as part of a protein complex containing Mte1. Consistent with this notion, deletion of *MTE1* conferred sensitivity to phleomycin that was similar to that conferred by deletion of *MPH1*, and the *mte1*Δ *mph1*Δ double mutant was no more sensitive, indicating that the genes function in the same genetic pathway for phleomycin resistance.

Our data suggest that Mte1 is not simply a structural component of Mph1 complexes, as Mte1 appears to have little effect on Mph1 stability *in vivo*. Mte1 could presumably play a role in targeting Mph1 to specific substrates *in vivo*. Such a role would be consistent with our findings that Mph1 nuclear foci and the recruitment or retention of Mph1 at double-strand breaks is compromised when Mte1 is absent. Mph1 suppresses cross-overs and break-induced replication by unwinding D-loop recombination intermediates (Mazon and Symington 2013; Prakash *et al.* 2009; Stafa *et al.* 2014). We find that Mte1 suppresses break-induced replication much like Mph1, thus it is also possible that Mte1 facilitates some aspect of Mph1 catalysis. Mte1 lacks obvious catalytic domains, and purified Mph1 is capable of unwinding D-loops and extended D-loops *in vitro* in the absence of Mte1 (Prakash *et al.* 2009; Sebesta *et al.* 2011; Sun *et al.* 2008). Nonetheless, it will be of great interest to determine whether Mte1 modulates Mph1 activity *in vitro*, as it appears that *in vivo* Mph1 is normally assembled into complexes that contain Mte1.

Orthologues of Mte1

Mte1 has readily identifiable orthologues in other yeasts, including *Kluveromyces*, *Candida*, *Pichia*, and *Ashbya* species. Mte1 appears to be an orthologue of the *Schizosaccharomyces pombe* Dbl2 protein (Yu *et al.* 2013). Dbl2 colocalizes with the fission yeast Rad52, and with double-strand breaks, and is important for nuclear focus formation by Fml1, the fission yeast orthologue of Mph1 (Yu *et al.* 2013). Dbl2 does not have a clear role in Fml1 inhibition of cross-overs or inhibition of BIR as of yet, so it is not known if Dbl2 plays a functional role similar to Mte1. Mte1 contains a domain of unknown function, DUF2439, that is found in the human ZGRF1 protein. The DUF2439 domain is also found in Dbl2 (Yu *et al.* 2013), but does not appear to be important for DNA damage resistance or for nuclear focus formation. Further, ZGRF1 is likely membrane-anchored and so might not be a true orthologue of Mte1. Nonetheless, as several lines of evidence suggest that Mph1 is an orthologue of the human FANCM protein (Whitby 2010), our evidence that Mph1 functions in concert with an important cofactor suggests that FANCM might also require a protein partner for effective function *in vivo*.

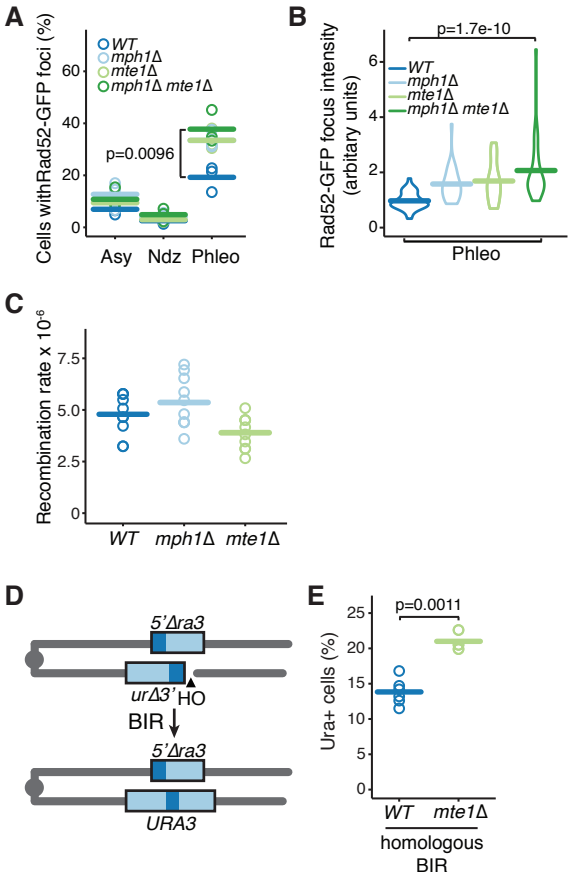

Figure 6 Mte1 contributes to double-strand break repair. (A) The percent of cells with Rad52 foci is plotted for the indicated strains. Samples were from logarithmic phase (Asy), G2/M (Ndz), and after treatment with 50 μg/ml phleomycin for 30 minutes (Phleo). Three replicates for each strain, for each condition, are plotted. The bars show the mean of the 3 replicates. N ranged from 42 to 160 cells per strain per replicate. The indicated samples were compared using a one-sided t-test. (B) The distribution of Rad52 focus intensity is plotted for the indicated strains, after treatment with 50 μg/ml phleomycin for 30 minutes (Phleo). The width of the box indicates the number of foci with a given intensity, and the bar indicates the mean. N=30 for all samples. The distributions were compared using the Wilcoxon rank sum test. (C) The direct repeat recombination rate was measured for the indicated strains. Each assay was a fluctuation test of nine cultures. The bars show the means of 10 replicates. (D) Schematic of the strain used to measure BIR. A DSB is induced by expression of the HO endonuclease. The right arm of chromosome III invades the left arm, and replication restores a functional *URA3* gene. (E) BIR was quantified for wild type and *mte1*Δ strains. N ranged from 3 to 6. The bars show the means of the replicates, and strains were compared using a t-test.

Acknowledgments

We thank members of the laboratories of Brenda Andrews and Charlie Boone for assistance with microscopy, and Tobit Glenhaber and Linus Glenhaber for assistance in constructing *mte1* deletion strains to measure BIR efficiency. We also thank Lorraine Symington and Daniel Durocher for providing strains. This work was supported by grants from the Canadian Cancer Society Research Institute (Impact grant 702310 to GWB), the Cancer Research Society (to GWB), the Natural Sciences and Engineering Research Council of Canada (Discovery Grant grant 327612 to ZZ), and the National Institutes of Health (GM76020 to JEH).

Author contributions

AY: Designed and carried out the experiments, wrote the paper, edited the paper. TK: Analyzed ChIP-seq data, edited the paper. RA: Performed and analyzed BIR assays. SM: Performed recombination assays, edited the paper. JO: Performed recombination analysis, constructed strains. JEH: Edited the paper. ZZ: Analyzed ChIP-seq data, edited the paper. GWB: Designed the experiments, wrote the paper, edited the paper.

Conflict of Interest

The authors declare that they have no conflict of interest.

Literature Cited

Alvaro, D., M. Lisby, and R. Rothstein, Genome-wide analysis of Rad52 foci reveals diverse mechanisms impacting recombinationt. PLoS Genet **3**: e228.

Anand, R. P., O. Tsaponina, P. W. Greenwell, C. S. Lee, W. Du, T. D. Petes, and J. E. Haber, Chromosome rearrangements via template switching between diverged repeated sequencest. Genes Dev **28**: 2394–406.

Askree, S. H., T. Yehuda, S. Smolikov, R. Gurevich, J. Hawk, C. Coker, A. Krauskopf, M. Kupiec, and M. J. McEachern, A genome-wide screen for Saccharomyces cerevisiae deletion mutants that affect telomere lengtht. Proc Natl Acad Sci U S A **101**: 8658–63.

Balint, A., T. Kim, D. Gallo, J. R. Cussiol, F. M. Bastos de Oliveira, A. Yimit, J. Ou, R. Nakato, A. Gurevich, K. Shirahige, M. B. Smolka, Z. Zhang, and G. W. Brown, Assembly of Slx4 signaling complexes behind DNA replication forkst. EMBO J **34**: 2182–97.

Banerjee, S., S. Smith, J. H. Oum, H. J. Liaw, J. Y. Hwang, N. Sikdar, A. Motegi, S. E. Lee, and K. Myung, Mph1p promotes gross chromosomal rearrangement through partial inhibition of homologous recombinationt. J Cell Biol **181**: 1083–93.

Blanco, M. G., J. Matos, U. Rass, S. C. Ip, and S. C. West, Functional overlap between the structure-specific nucleases Yen1 and Mus81-Mms4 for DNA-damage repair in S. cerevisiaet. DNA Repair (Amst) **9**: 394–402.

Brachmann, C. B., A. Davies, G. J. Cost, E. Caputo, J. Li, P. Hieter, and J. D. Boeke, Designer deletion strains derived from Saccharomyces cerevisiae S288C: a useful set of strains and plasmids for PCR-mediated gene disruption and other applicationst. Yeast **14**: 115–32.

Burgess, R. C., M. Lisby, V. Altmannova, L. Krejci, P. Sung, and R. Rothstein, Localization of recombination proteins and Srs2 reveals anti-recombinase function in vivot. J Cell Biol **185**: 969–81.

Chavez, A., V. Agrawal, and F. B. Johnson, Homologous recombination-dependent rescue of deficiency in the structural maintenance of chromosomes (Smc) 5/6 complext. J Biol Chem **286**: 5119–25.

Chen, Y. H., K. Choi, B. Szakal, J. Arenz, X. Duan, H. Ye, D. Branzei, and X. Zhao, Interplay between the Smc5/6 complex and the Mph1 helicase in recombinational repairt. Proc Natl Acad Sci U S A **106**: 21252–7.

Chen, Y. H., B. Szakal, F. Castellucci, D. Branzei, and X. Zhao, DNA damage checkpoint and recombinational repair differentially affect the replication stress tolerance of Smc6 mutantst. Mol Biol Cell **24**: 2431–41.

Cherry, J. M., E. L. Hong, C. Amundsen, R. Balakrishnan, G. Binkley, E. T. Chan, K. R. Christie, M. C. Costanzo, S. S. Dwight, S. R. Engel, D. G. Fisk, J. E. Hirschman, B. C. Hitz, K. Karra, C. J. Krieger, S. R. Miyasato, R. S. Nash, J. Park, M. S. Skrzypek, M. Simison, S. Weng, and E. D. Wong, Saccharomyces Genome Database: the genomics resource of budding yeastt. Nucleic Acids Res **40**: D700–5.

Choi, K., B. Szakal, Y. H. Chen, D. Branzei, and X. Zhao, The Smc5/6 complex and Esc2 influence multiple replication-associated recombination processes in Saccharomyces cerevisiaet. Mol Biol Cell **21**: 2306–14.

Denervaud, N., J. Becker, R. Delgado-Gonzalo, P. Damay, A. S. Rajkumar, M. Unser, D. Shore, F. Naef, and S. J. Maerkl, A chemostat array enables the spatio-temporal analysis of the yeast proteomet. Proc Natl Acad Sci U S A **110**: 15842–7.

Engel, S. R., F. S. Dietrich, D. G. Fisk, G. Binkley, R. Balakrishnan, M. C. Costanzo, S. S. Dwight, B. C. Hitz, K. Karra, R. S. Nash, S. Weng, E. D. Wong, P. Lloyd, M. S. Skrzypek, S. R. Miyasato, M. Simison, and J. M. Cherry, The reference genome sequence of Saccharomyces cerevisiae: then and nowt. G3 (Bethesda) **4**: 389–98.

Entian, K. D., T. Schuster, J. H. Hegemann, D. Becher, H. Feldmann, U. Guldener, R. Gotz, M. Hansen, C. P. Hollenberg, G. Jansen, W. Kramer, S. Klein, P. Kotter, J. Kricke, H. Launhardt, G. Mannhaupt, A. Maierl, P. Meyer, W. Mewes, T. Munder, R. K. Niedenthal, M. Ramezani Rad, A. Rohmer, A. Romer, A. Hinnen, and et al., Functional analysis of 150 deletion mutants in Saccharomyces cerevisiae by a systematic approacht. Mol Gen Genet **262**: 683–702.

Ferrari, M., D. Dibitetto, G. De Gregorio, V. V. Eapen, C. C. Rawal, F. Lazzaro, M. Tsabar, F. Marini, J. E. Haber, and A. Pellicioli, Functional interplay between the 53BP1-ortholog Rad9 and the Mre11 complex regulates resection, end-tethering and repair of a double-strand breakt. PLoS Genet **11**: e1004928.

Gallina, I., C. Colding, P. Henriksen, P. Beli, K. Nakamura, J. Offman, D. P. Mathiasen, S. Silva, E. Hoffmann, A. Groth, C. Choudhary, and M. Lisby, Cmr1/WDR76 defines a nuclear genotoxic stress body linking genome integrity and protein quality controlt. Nat Commun **6**: 6533.

Germann, S. M., V. H. Oestergaard, C. Haas, P. Salis, A. Motegi, and M. Lisby, Dpb11/TopBP1 plays distinct roles in DNA replication, checkpoint response and homologous recombinationt. DNA Repair (Amst) **10**: 210–24.

Ho, C. K., G. Mazon, A. F. Lam, and L. S. Symington, Mus81 and Yen1 promote reciprocal exchange during mitotic recombination to maintain genome integrity in budding yeastt. Mol Cell **40**: 988–1000.

Huh, W. K., J. V. Falvo, L. C. Gerke, A. S. Carroll, R. W. Howson, J. S. Weissman, and E. K. O'Shea, Global analysis of protein localization in budding yeastt. Nature **425**: 686–91.

Ivanov, E. L., N. Sugawara, C. I. White, F. Fabre, and J. E. Haber, Mutations in XRS2 and RAD50 delay but do not prevent mating-type switching in Saccharomyces cerevisiaet. Mol Cell Biol **14**: 3414–25.

Langmead, B. and S. L. Salzberg, Fast gapped-read alignment with Bowtie 2t. Nat Methods **9**: 357–9.

Lazzaro, F., V. Sapountzi, M. Granata, A. Pellicioli, M. Vaze, J. E. Haber, P. Plevani, D. Lydall, and M. Muzi-Falconi, Histone methyltransferase Dot1 and Rad9 inhibit single-stranded DNA accumulation at DSBs and uncapped telomerest. EMBO J **27**: 1502–12.

Lea, D. E. and C. A. Coulson, The Distribution of the Numbers of Mutants in Bacterial Populationst. Journal of Genetics **49**: 264–285.

Lisby, M., J. H. Barlow, R. C. Burgess, and R. Rothstein, Choreography of the DNA Damage Response; Spatiotemporal Relationships among Checkpoint and Repair Proteinst. Cell **118**: 699–713.

Lisby, M., U. H. Mortensen, and R. Rothstein, Colocalization of multiple DNA double-strand breaks at a single Rad52 repair centret. Nat Cell Biol **5**: 572–7.

Lisby, M., R. Rothstein, and U. H. Mortensen, Rad52 forms DNA repair and recombination centers during S phaset. Proc Natl Acad Sci U S A **98**: 8276–82.

Luke-Glaser, S. and B. Luke, The Mph1 helicase can promote telomere uncapping and premature senescence in budding yeastt. PLoS One **7**: e42028.

Mazon, G. and L. S. Symington, Mph1 and Mus81-Mms4 prevent aberrant processing of mitotic recombination intermediatest. Mol Cell **52**: 63–74.

Mazumder, A., L. Q. Pesudo, S. McRee, M. Bathe, and L. D. Samson, Genome-wide single-cell-level screen for protein abundance and localization changes in response to DNA damage in S. cerevisiaet. Nucleic Acids Res **41**: 9310–24.

Melo, J. A., J. Cohen, and D. P. Toczyski, Two checkpoint complexes are independently recruited to sites of DNA damage in vivot. Genes Dev. **15**: 2809–2821.

Pellicioli, A., C. Lucca, G. Liberi, F. Marini, M. Lopes, P. Plevani, A. Romano, P. P. Di Fiore, and M. Foiani, Activation of Rad53 kinase in response to DNA damage and its effect in modulating phosphorylation of the lagging strand DNA polymeraset. EMBO J **18**: 6561–72.

Prakash, R., L. Krejci, S. Van Komen, K. Anke Schurer, W. Kramer, and P. Sung, Saccharomyces cerevisiae MPH1 gene, required for homologous recombination-mediated mutation avoidance, encodes a 3′ to 5′ DNA helicaset. J Biol Chem **280**: 7854–60.

Prakash, R., D. Satory, E. Dray, A. Papusha, J. Scheller, W. Kramer, L. Krejci, H. Klein, J. E. Haber, P. Sung, and G. Ira, Yeast Mph1 helicase dissociates Rad51-made D-loops: implications for crossover control in mitotic recombinationt. Genes Dev **23**: 67–79.

Roberts, T. M., I. W. Zaidi, J. A. Vaisica, M. Peter, and G. W. Brown, Regulation of rtt107 recruitment to stalled DNA replication forks by the cullin rtt101 and the rtt109 acetyltransferaset. Mol Biol Cell **19**: 171–80.

Scheller, J., A. Schurer, C. Rudolph, S. Hettwer, and W. Kramer, MPH1, a yeast gene encoding a DEAH protein, plays a role in protection of the genome from spontaneous and chemically induced damaget. Genetics **155**: 1069–81.

Schurer, K. A., C. Rudolph, H. D. Ulrich, and W. Kramer, Yeast MPH1 gene functions in an error-free DNA damage bypass pathway that requires genes from Homologous recombination, but not from postreplicative repairt. Genetics **166**: 1673–86.

Sebesta, M., P. Burkovics, L. Haracska, and L. Krejci, Reconstitution of DNA repair synthesis in vitro and the role of polymerase and helicase activitiest. DNA Repair (Amst) **10**: 567–76.

Shimomura, T., S. Ando, K. Matsumoto, and K. Sugimoto, Functional and physical interaction between Rad24 and Rfc5 in the yeast checkpoint pathwayst. Mol Cell Biol **18**: 5485–91.

Smith, J. and R. Rothstein, An allele of RFA1 suppresses RAD52-dependent double-strand break repair in Saccharomyces cerevisiaet. Genetics **151**: 447–58.

Stafa, A., R. A. Donnianni, L. A. Timashev, A. F. Lam, and L. S. Symington, Template switching during break-induced replication is promoted by the Mph1 helicase in Saccharomyces cerevisiaet. Genetics **196**: 1017–28.

Sugawara, N., X. Wang, and J. E. Haber, In vivo roles of Rad52, Rad54, and Rad55 proteins in Rad51-mediated recombinationt. Mol Cell **12**: 209–19.

Sun, W., S. Nandi, F. Osman, J. S. Ahn, J. Jakovleska, A. Lorenz, and M. C. Whitby, The FANCM ortholog Fml1 promotes recombination at stalled replication forks and limits crossing over during DNA double-strand break repairt. Mol Cell **32**: 118–28.

Symington, L. S., Role of RAD52 epistasis group genes in homologous recombination and double-strand break repairt. Microbiol Mol Biol Rev **66**: 630–70, table of contents.

Szostak, J. W., T. L. Orr-Weaver, R. J. Rothstein, and F. W. Stahl, The double-strand-break repair model for recombinationt. Cell **33**: 25–35.

Tkach, J. M., A. Yimit, A. Y. Lee, M. Riffle, M. Costanzo, D. Jaschob, J. A. Hendry, J. Ou, J. Moffat, C. Boone, T. N. Davis, C. Nislow, and G. W. Brown, Dissecting DNA damage response pathways by analysing protein localization and abundance changes during DNA replication stresst. Nat Cell Biol **14**: 966–76.

Tsabar, M., V. V. Eapen, J. M. Mason, G. Memisoglu, D. P. Waterman, M. J. Long, D. K. Bishop, and J. E. Haber, Caffeine impairs resection during DNA break repair by reducing the levels of nucleases Sae2 and Dna2t. Nucleic Acids Res **43**: 6889–901.

Whitby, M. C., The FANCM family of DNA helicases/translocasest. DNA Repair (Amst) **9**: 224–36.

Wolner, B., S. van Komen, P. Sung, and C. L. Peterson, Recruitment of the recombinational repair machinery to a DNA double-strand break in yeastt. Mol Cell **12**: 221–32.

Wu, L., C. Z. Bachrati, J. Ou, C. Xu, J. Yin, M. Chang, W. Wang, L. Li, G. W. Brown, and I. D. Hickson, BLAP75/RMI1 promotes the BLM-dependent dissolution of homologous recombination intermediatest. Proc Natl Acad Sci U S A **103**: 4068–73.

Wu, L. and I. D. Hickson, The Bloom's syndrome helicase suppresses crossing over during homologous recombinationt. Nature **426**: 870–4.

Xue, X., K. Choi, J. Bonner, T. Chiba, Y. Kwon, Y. Xu, H. Sanchez, C. Wyman, H. Niu, X. Zhao, and P. Sung, Restriction of replication fork regression activities by a conserved SMC complext. Mol Cell **56**: 436–45.

Yang, J., C. Z. Bachrati, J. Ou, I. D. Hickson, and G. W. Brown, Human topoisomerase IIIalpha is a single-stranded DNA decatenase that is stimulated by BLM and RMI1t. J Biol Chem **285**: 21426–36.

Yu, Y., J. Y. Ren, J. M. Zhang, F. Suo, X. F. Fang, F. Wu, and L. L. Du, A proteome-wide visual screen identifies fission yeast proteins localizing to DNA double-strand breakst. DNA Repair (Amst) **12**: 433–43.

Zheng, X. F., R. Prakash, D. Saro, S. Longerich, H. Niu, and P. Sung, Processing of DNA structures via DNA unwinding and branch migration by the S. cerevisiae Mph1 proteint. DNA Repair (Amst) **10**: 1034–43.

Zhu, Z., W. H. Chung, E. Y. Shim, S. E. Lee, and G. Ira, Sgs1 helicase and two nucleases Dna2 and Exo1 resect DNA double-strand break endst. Cell **134**: 981–994.

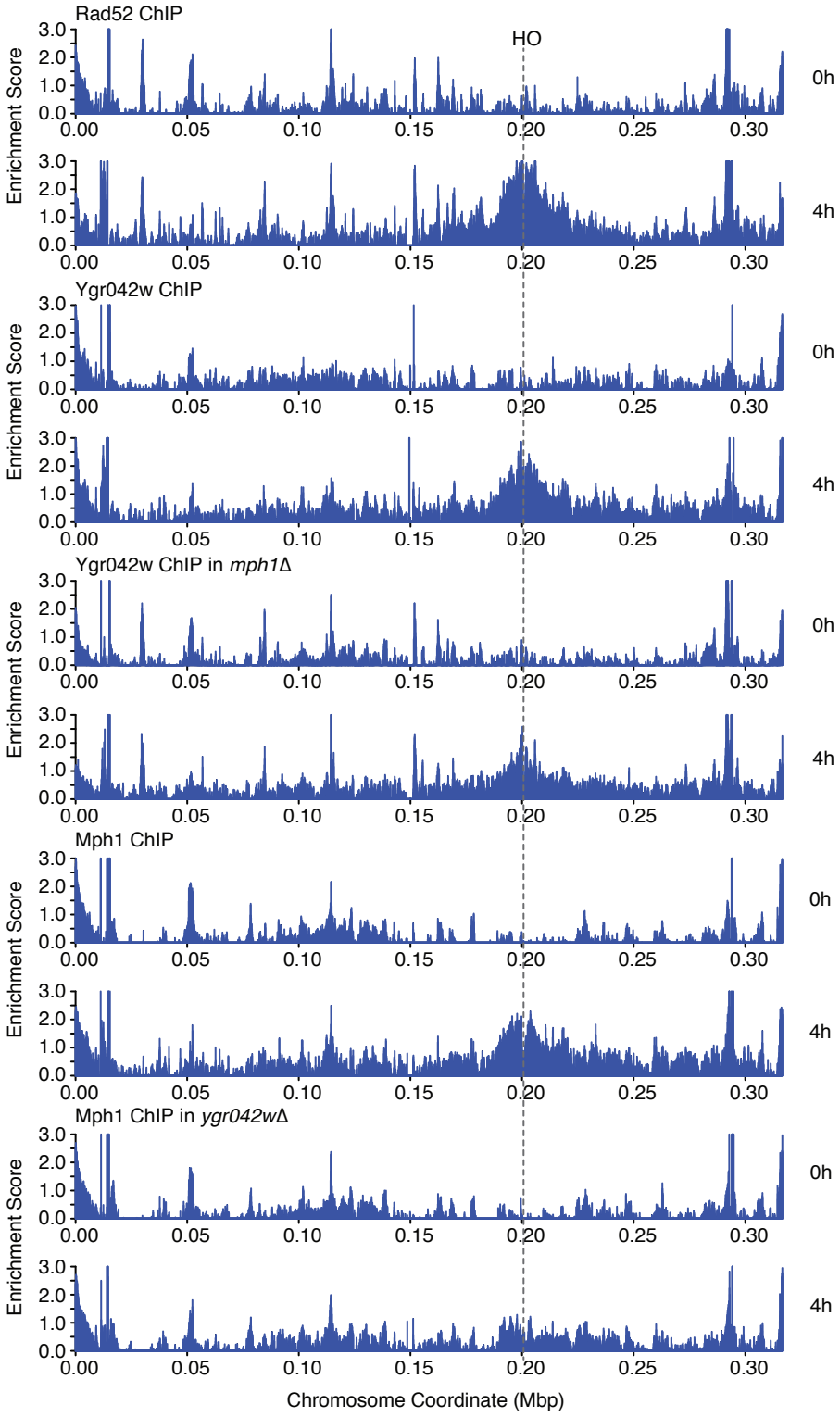

Figure S1. Mte1 and Mph1 are recruited to double-strand DNA breaks. ChIP-seq analysis was performed on *RAD52-FLAG*, *MTE1-FLAG*, *MTE1-FLAG mph1*Δ, *MPH1-FLAG*, and *MPH1-FLAG mte1*Δ cells at 0h and 4h following the induction of a specific double-strand break at the MAT locus by the HO endonuclease. ChIP enrichment scores representing the log2 immunoprecipitate to input ratio are plotted across chromosome III for each time point. The position of the HO cut site is indicated.

Table S1. Yeast Strains used in this study.

Strain	Genotype	Source
GFP collection	*MAT***a** *xxx-GFP::HIS3MX ura3Δ0 leu2Δ0 his3Δ1 met15Δ0*	Huh *et al, 2003*
AYY38	*MATα RAD52-yEmRFP::CaURA3 can1Δ::STE2pr-LEU2 leu2Δ0 his3Δ1 ura3Δ0 met15Δ0 lyp1Δ*	this study
AYY110	*MATα MTE1-GFP::HIS3MX can1Δ::STE2pr-LEU2 NUP49-mCherry::CaURA3 leu2Δ0 his3Δ1 ura3Δ0 met15Δ0 lyp1Δ*	this study
AYY80	*MAT***a** *mte1Δ::kanMX ura3Δ0 leu2Δ0 his3Δ1 met15Δ0*	this study
Deletion collection	*MAT***a** *xxx::kanMX ura3Δ0 leu2Δ0 his3Δ1 met15Δ0*	Giaever *et al*, 2002
AYY73	*MAT***a** *MTE1-GFP::kanMX ura3Δ0 leu2Δ0 his3Δ1 met15Δ0*	this study
AYY56	*MAT***a** *MTE1-GFP::HIS3MX mec1Δ::LEU2 sml1::kanMX leu2Δ0 his3Δ1 ura3Δ0 met15Δ0*	this study
AYY57	*MAT***a** *MTE1-GFP::HIS3MX tel1Δ::natMX leu2Δ0 his3Δ1 ura3Δ0*	this study
AYY76	*MAT***a** *MTE1-GFP::HIS3MX mec1Δ::LEU2 tel1Δ::natMX sml1Δ::kanMX leu2Δ0 his3Δ1 ura3Δ0*	this study
	*MAT***a** *MTE1-GFP::kanMX rad52Δ::natMX leu2Δ0 his3Δ1 ura3Δ0 met15Δ0 can1Δ::STE2pr-LEU2*	this study
	*MAT***a** *MTE1-GFP::kanMX mre11Δ::natMX leu2Δ0 his3Δ1 ura3Δ0 met15Δ0 can1Δ::STE2pr-LEU2*	this study
	*MAT***a** *MTE1-GFP::kanMX rad50Δ::natMX leu2Δ0 his3Δ1 ura3Δ0 met15Δ0 can1Δ::STE2pr-LEU2*	this study
	*MAT***a** *MTE1-GFP::kanMX xrs2Δ::natMX leu2Δ0 his3Δ1 ura3Δ0 met15Δ0 can1Δ::STE2pr-LEU2*	this study
	*MAT***a** *MTE1-GFP::kanMX rad9Δ::natMX leu2Δ0 his3Δ1 ura3Δ0 met15Δ0 can1Δ::STE2pr-LEU2*	this study
	*MAT***a** *MTE1-GFP::kanMX mph1Δ::natMX ura3Δ0 leu2Δ0 his3Δ1 met15Δ0 can1Δ::STE2pr-LEU2*	this study
Y1429	*MATα rfa2-ph::natMX can1Δ::STE2pr-Sphis5 leu2Δ0 his3Δ1 ura3Δ0 met15Δ0 lyp1Δ*	C. Boone
	*MAT***a** *MTE1-GFP::kanMX mgs1Δ::natMX leu2Δ0 his3Δ1 ura3Δ0 met15Δ0*	this study
	*MAT***a** *MTE1-GFP::kanMX rfa2-ph::natMX leu2Δ0 his3Δ1 ura3Δ0 met15Δ0*	this study
AYY85	*MAT***a** *MPH1-GFP::HIS3MX ura3Δ0 leu2Δ0 his3Δ1 met15Δ0*	this study
AYY107	*MAT***a** *MPH1-GFP::HIS3MX mte1Δ::kanMX can1Δ::STE2pr-LEU2 RPL39pr-TdTomato::CaURA3 leu2Δ0 his3Δ ura3Δ0 lyp1Δ*	this study
AYY75	*MAT***a** *MTE1-6His10flag::kanMX ura3Δ0 leu2Δ0 his3Δ1 met15Δ0*	this study
AYY139	*MAT***a** *MPH1-3HA::HIS3MX MTE1-6His10flag::kanMX his3Δ1 leuΔ0 ura3Δ0 met15Δ0*	this study
AYY92	*MAT***a** *mte1Δ::kanMX rad52Δ::natMX can1Δ::STE2pr-LEU2 leu2Δ0 his3Δ1 ura3Δ0 met15Δ0 lyp1Δ*	this study
AYY112	*MAT***a** *mte1Δ::kanMX mph1Δ::natMX leu2Δ0 his3Δ1 ura3Δ0*	this study
	MATα rad52Δ::natMX can1Δ::STE2pr-LEU2 leu2Δ0 his3Δ1 ura3Δ0 met15Δ0 lyp1Δ	C. Boone
	*MAT***a** *mph1Δ::natMX leu2Δ0 his3Δ1 ura3Δ0 met15Δ0 lyp1Δ*	this study
AYY182	*MATα RAD52-6His10flag::kanMX hoΔ hml::ADE1 hmr::ADE1 ade1 leu2-3,112 trp1::hisG lys5 ura3-52 ade3::GAL1pr-HO*	this study
AYY140	*MATα MTE1-6His10flag::kanMX hoΔ hml::ADE1 hmr::ADE1 ade1 leu2-3,112 trp1::hisG lys5 ura3-52 ade3::GAL1pr-HO*	this study
AYY148	*MATα MTE1-6his10flag::kanMX mph1Δ::natMX hoΔ hml::ADE1 hmr::ADE1 ade1 leu2-3,112 trp1::hisG lys5 ura3-52 ade3::GAL1pr-HO*	this study
AYY156	*MATα MPH1-6his10flag::kanMX hoΔ hml::ADE1 hmr::ADE1 ade1 leu2-3,112 trp1::hisG lys5 ura3-52 ade3::GAL1pr-HO*	this study
AYY155	*MATα MPH1-6his10flag::kanMX mte1Δ::natMX hoΔ hml::ADE1 hmr::ADE1 ade1 leu2-3,112 trp1::hisG lys5 ura3-52 ade3::GAL1pr-HO*	this study
AYY116	*MAT***a** *RAD52-GFP::HIS3MX mte1Δ::kanMX leu2Δ0 his3Δ ura3Δ0 lys2Δ0*	this study
AYY117	*MAT***a** *RAD52-GFP::HIS3MX mph1Δ::natMX leu2Δ0 his3Δ ura3Δ0 lys2Δ0*	this study
AYY118	*MAT***a** *RAD52-GFP::HIS3MX mte1Δ::kanMX mph1Δ::natMX leu2Δ0 his3Δ ura3Δ0 lys2Δ0*	this study
JOY90	*MATα mfa1Δ::MFA1pr-HIS3 leu2ΔEcoRI::URA3-HOcs::leu2ΔBstEII leu2Δ0 his3Δ1 ura3Δ0 met15Δ0 lyp1Δ can1Δ:::natMX*	this study
AYY119	*MATα mte1Δ::kanMX leu2ΔEcoRI::URA3-HOcs::leu2ΔBstEII leu2Δ0 his3Δ1 ura3Δ0 met15Δ0 lyp1Δ can1Δ:::natMX*	this study
AYY120	*MATα mph1Δ::kanMX leu2ΔEcoRI::URA3-HOcs::leu2ΔBstEII leu2Δ0 his3Δ1 ura3Δ0 met15Δ0 lyp1Δ can1Δ:::natMX*	this study
yRA253	*MAT***a***ΔHOcs::hisG ura3Δ851 trp1Δ63 leu2Δ::kanMX hmlΔ::hisG hmrΔ::ADE3 ade3::GAL1pr-HO can1Δ::URdonor-Hocs-natMX acceptorA3::TRP1*	this study
yRA276	*MAT***a***ΔHOcs::hisG ura3Δ851 trp1Δ63 leu2Δ::kanMX hmlΔ::hisG hmrΔ::ADE3 ade3::GAL1pr-HO can1Δ::URdonor-Hocs-natMX acceptorA3::TRP1 mte1Δ::hph*	this study
BY4741	*MAT***a** *his3Δ leu2Δ ura3Δ met15Δ*	Brachmann *et al.* 1998

References

Brachmann CB, Davies A, Cost GJ, Caputo E, Li J, Hieter P, and Boeke JD (1998). Designer deletion strains derived from Saccharomyces cerevisiae S288C: a useful set of strains and plasmids for PCR-mediated gene disruption and other applications. Yeast **14:** 115-132.

Giaever G, Chu AM, Ni L, Connelly C, Riles L, Veronneau S, Dow S, Lucau-Danila A, Anderson K, Andre B, *et al.* (2002). Functional profiling of the Saccharomyces cerevisiae genome. Nature **418:** 387-391.

Huh WK, Falvo JV, Gerke LC, Carroll AS, Howson RW, Weissman JS, and O'Shea EK (2003). Global analysis of protein localization in budding yeast. Nature **425:** 686-691.

Table S2. ChIP-seq statistics

Genotype	Strain	Condition	Sample Title	Sample Type	Sample Name	Sequencing Type	# of reads	Sequencing Coverage	Alignment Rate	SRA Accession Number
RAD52-FLAG	AYY182	0h + gal	15-06-10_1st_ay_w303_Rad52flag_WT_0h_input_S-50-H	Input	AY1	Single-end (50 bp)	18053040	73	97.18%	SRR2559330
RAD52-FLAG	AYY182	0h + gal	15-06-10_1st_ay_w303_Rad52flag_WT_0h_ChIP_S-50-H	ChIP	AY2	Single-end (50 bp)	19286579	79	97.72%	SRR2559331
RAD52-FLAG	AYY182	4h + gal	15-06-10_1st_ay_w303_Rad52flag_WT_4h_input_S-50-H	Input	AY3	Single-end (50 bp)	23173512	94	97.33%	SRR2559343
RAD52-FLAG	AYY182	4h + gal	15-06-10_1st_ay_w303_Rad52flag_WT_4h_ChIP_S-50-H	ChIP	AY4	Single-end (50 bp)	19323387	79	97.65%	SRR2559344
MTE1-FLAG	AYY140	0h + gal	15-06-10_1st_ay_w303_YGR042wflag_WT_0h_input_S-50-H	Input	AY5	Single-end (50 bp)	18493194	91	97.58%	SRR2559345
MTE1-FLAG	AYY140	0h + gal	15-06-10_1st_ay_w303_YGR042Wflag_WT_0h_ChIP_S-50-H	ChIP	AY6	Single-end (50 bp)	22666774	76	96.22%	SRR2559346
MTE1-FLAG	AYY140	4h + gal	15-06-10_1st_ay_w303_YGR042wflag_WT_4h_input_S-50-H	Input	AY7	Single-end (50 bp)	17839811	72	97.12%	SRR2559347
MTE1-FLAG	AYY140	4h + gal	15-06-10_1st_ay_w303_YGR042Wflag_WT_4h_ChIP_S-50-H	ChIP	AY8	Single-end (50 bp)	15075923	62	97.50%	SRR2559348
MTE1-FLAG mph1Δ	AYY148	0h + gal	15-06-10_1st_ay_w303_YGR042wflag_mph1Δ_0h_input_S-50-H	Input	AY9	Single-end (50 bp)	25713709	105	97.27%	SRR2559349
MTE1-FLAG mph1Δ	AYY148	0h + gal	15-06-10_1st_ay_w303_YGR042Wflag_mph1Δ_0h_ChIP_S-50-H	ChIP	AY10	Single-end (50 bp)	12812434	53	97.63%	SRR2559350
MTE1-FLAG mph1Δ	AYY148	4h + gal	15-06-10_1st_ay_w303_YGR042wflag_mph1Δ_4h_input_S-50-H	Input	AY11	Single-end (50 bp)	14973419	61	97.03%	SRR2559333
MTE1-FLAG mph1Δ	AYY148	4h + gal	15-06-10_1st_ay_w303_YGR042Wflag_mph1Δ_4h_ChIP_S-50-H	ChIP	AY12	Single-end (50 bp)	12793985	52	97.46%	SRR2559334
MPH1-FLAG mte1Δ	AYY155	0h + gal	15-06-10_1st_ay_w303_Mph1flag_ygr042wΔ_0h_input_S-50-H	Input	AY13	Single-end (50 bp)	17581434	71	96.82%	SRR2559335
MPH1-FLAG mte1Δ	AYY155	0h + gal	15-06-10_1st_ay_w303_Mph1flag_ygr042wΔ_0h_ChIP_S-50-H	ChIP	AY14	Single-end (50 bp)	14024187	57	97.36%	SRR2559336
MPH1-FLAG mte1Δ	AYY155	4h + gal	15-06-10_1st_ay_w303_Mph1flag_ygr042wΔ_4h_input_S-50-H	Input	AY15	Single-end (50 bp)	13983994	57	97.25%	SRR2559337
MPH1-FLAG mte1Δ	AYY155	4h + gal	15-06-10_1st_ay_w303_Mph1flag_ygr042wΔ_4h_ChIP_S-50-H	ChIP	AY16	Single-end (50 bp)	12879861	52	97.13%	SRR2559338
MPH1-FLAG	AYY156	0h + gal	15-06-10_1st_ay_w303_Mph1flag_WT_0h_input_S-50-H	Input	AY17	Single-end (50 bp)	17363022	71	97.34%	SRR2559339
MPH1-FLAG	AYY156	0h + gal	15-06-10_1st_ay_w303_Mph1flag_WT_0h_ChIP_S-50-H	ChIP	AY18	Single-end (50 bp)	13779730	56	96.81%	SRR2559340
MPH1-FLAG	AYY156	4h + gal	15-06-10_1st_ay_w303_Mph1flag_WT_4h_input_S-50-H	Input	AY19	Single-end (50 bp)	15831080	64	97.04%	SRR2559341
MPH1-FLAG	AYY156	4h + gal	15-06-10_1st_ay_w303_Mph1flag_WT_4h_ChIP_S-50-H	ChIP	AY20	Single-end (50 bp)	12284973	50	97.57%	SRR2559342

Table S3. GFP fusion proteins that co-localize with Rad52 during phleomycin treatment (percent of foci)

GFP-protein	ORF	% of GFP-Xxx foci that overlap Rad52 foci	% of Rad52 foci that overlap GFP-Xxx foci	# of Rad52-RFP foci	# of Xxx-GFP foci	Number of cells	Previously described co-localization with Rad52
Srs2	YJL092W	78.9	29.4	51	19	201	yes[a]
Rad59	YDL059C	54.5	30.0	20	11	147	yes[b]
Ygr042w	YGR042W	54.4	46.8	158	136	889	
Rad57	YDR004W	53.3	9.8	82	15	216	
Rad55	YDR076W	52.6	23.3	43	19	315	
Ddc2	YDR499W	47.1	71.4	91	138	197	yes[b]
Mgs1	YNL218W	43.2	35.6	90	74	482	
Dna2	YHR164C	40.7	61.2	139	209	641	yes[b]
Top3	YLR234W	37.5	12.5	24	8	185	
Rad53	YPL153C	34.8	25.0	96	69	329	
Rfa1	YAR007C	34.5	78.4	37	84	103	yes[c]
Rad9	YDR217C	34.0	39.5	43	50	227	yes[b]
Dpb11	YJL090C	31.3	57.7	26	48	102	yes[d]
Rmi1	YPL024W	30.4	12.1	58	23	318	
Rad54	YGL163C	30.2	30.2	43	43	166	yes[b]
Rfa2	YNL312W	27.4	65.4	26	62	59	yes[b]
Sgs1	YMR190C	26.3	12.5	40	19	162	
Ddc1	YPL194W	24.3	71.4	35	103	118	yes[b]
Rtt107	YHR154W	18.8	26.1	23	32	131	
Rad24	YER173W	17.6	2.0	153	17	430	
Rdh54	YBR073W	16.3	31.3	67	129	402	
Slx4	YLR135W	14.0	30.8	26	57	169	
Rtt101	YJL047C	12.5	4.5	111	40	563	
Mms21	YEL091C	9.3	8.0	50	43	258	
Mre11	YMR224C	9.1	7.7	39	33	123	yes[b]
Slx8	YER116C	8.0	3.1	64	25	281	
Rad5	YLR032W	7.0	5.0	80	57	676	
Rad50	YNL250W	4.0	3.6	55	50	244	
Csm1	YCR086W	1.7	1.6	63	60	269	

a. Burgess, R.C., Lisby M., Altmannova V., Krejci L., Sung P., and Rothstein R, 2009 Localization of recombination proteins and Srs2 reveals anti-recombinase function in vivo. The Journal of Cell Biology 185(6):969-981

b. Lisby, M., J.H. Barlow, R.C. Burgess, and R. Rothstein, 2004 Choreography of the DNA Damage Response; Spatiotemporal Relationships among Checkpoint and Repair Proteins. Cell 118 (6):699-713

c. Zhu, Z., Chung, W.H., Shim, E.Y., Lee, S.E., Ira, G, 2008 Sgs1 helicase and two nucleases Dna2 and Exo1 resect DNA double-strand break ends. Cell 134(6): 981-994

d. Germann, S.M., Oestergaad, V.H., Haas, C., Salis, P., Motegi, A., and Lisby, M, 2011 Dpb11/TopBP1 plays distinct roles in DNA replication, checkpoint response and homologous recombination. DNA Repair (Amst) 10(2):210-224

Pink shading indicates Xxx-GFP co-localizations less frequent than Mre11-GFP, and so should be regarded with caution.

Table S4. GFP fusion proteins that co-localize with Rad52 during phleomycin treatment (percent of cells)

GFP-protein	ORF	Number of cells	Percent of cells with Rad52-RFP foci	Percent of cells with Xxx-GFP foci	Percent of cells with co-localized foci
Ddc1	YPL194W	197	8.6	24.9	27.4
Rfa1	YAR007C	103	7.8	36.9	24.3
Rfa2	YNL312W	59	13.6	39.0	22.0
Ddc2	YDR499W	118	5.9	39.0	19.5
Dpb11	YJL090C	102	5.9	28.4	13.7
Dna2	YHR164C	641	5.0	14.2	12.5
Ygr042w	YGR042W	889	9.0	6.0	7.5
Rad9	YDR217C	227	11.0	13.2	7.5
Srs2	YJL092W	201	16.4	2.0	7.5
Rad53	YPL153C	329	17.9	14.9	6.7
Rad54	YGL163C	166	16.9	14.5	6.6
Mgs1	YNL218W	482	10.6	7.3	5.8
Rdh54	YBR073W	402	10.2	23.4	5.0
Rtt107	YHR154W	131	13.0	16.0	4.6
Slx4	YLR135W	169	10.7	23.1	4.1
Rad59	YDL059C	147	7.5	3.4	4.1
Rad57	YDR004W	216	27.8	2.8	3.7
Rad55	YDR076W	315	9.8	2.9	3.2
Top3	YLR234W	162	19.8	8.6	3.1
Mre11	YMR224C	123	23.6	21.1	2.4
Rmi1	YPL024W	318	14.2	4.1	2.2
Sgs1	YMR190C	185	10.8	2.7	1.6
Mms21	YEL091C	258	17.4	15.1	1.6
Rtt101	YJL047C	563	18.7	6.0	0.9
Rad50	YNL250W	244	19.3	16.4	0.8
Slx8	YER116C	281	19.9	7.1	0.7
Rad5	YLR032W	676	10.1	7.0	0.6
Rad24	YER173W	430	28.4	3.3	0.5
Csm1	YCR086W	269	21.9	23.8	0.4

Table S5. GFP fusion proteins that do not co-localize with Rad52 during phleomycin treatment (percent of cells)

GFP-protein	ORF	Number of cells	Percent of cells with Rad52-RFP foci	Percent of cells with Xxx-GFP foci	Number of Xxx-GFP foci	Percent of cells with co-localized foci
Oaf3	YKR064W	179	31.8	48.0	104	0
Yku70	YMR284W	335	18.2	24.5	100	0
Atg29	YPL166W	152	44.1	46.7	82	0
Crm1	YGR218W	206	19.9	25.7	78	0
Tub1	YML085C	235	20.4	17.0	37	0
Rrb1	YMR131C	255	15.3	12.2	32	0
Cdc27	YBL084C	189	8.7	7.2	31	0
Ymr111c	YMR111C	116	25.0	23.3	31	0
Pso2	YMR137C	356	23.3	7.9	30	0
Mrt4	YKL009W	132	23.5	17.4	23	0
Cgr1	YGL029W	164	21.3	10.4	17	0
Lsb1	YGR136W	227	30.8	5.3	15	0
Mrc1	YCL061C	261	25.7	5.4	15	0
Pph21	YDL134C	228	28.1	4.4	14	0
Tof2	YKR010C	109	11.9	11.9	14	0
Xrs2	YDR369C	280	10.7	5.0	14	0
Dus3	YLR401C	248	29.0	4.0	11	0
Pph3	YDR075W	201	20.4	5.0	9	0
Hta2	YBL003C	325	11.7	2.8	9	0
Edc2	YER035W	250	24.0	4.0	8	0
Ylr363w-a	YLR363W-A	180	27.8	4.4	8	0
Hos2	YGL194C	207	28.0	3.4	7	0
Apj1	YNL077W	186	24.2	3.2	6	0
Csm3	YMR048W	138	52.2	3.6	6	0
Rfc2	YJR068W	224	23.7	2.2	5	0
Ylr126c	YLR126C	193	23.8	4.1	5	0
Dug2	YBR281C	104	19.2	3.8	4	0
Rfc3	YNL290W	198	18.2	1.5	4	0
Rps18A	YDR450W	216	14.4	0.9	2	0
Pph22	YDL188C	248	21.8	0.8	2	0
Rfc5	YBR087W	199	39.7	0.5	1	0
Cmr1	YDL156W	198	25.3	0.0	0	0[a]

[a] No Xxx-GFP foci were detected.

Table S6. Mutants that affect Mte1-GFP focus formation

Standard Name	Systematic Name	Result		Confirmed in quantitative analysis
		Control	2 hours + phleo	
MGS1	YNL218W	unchanged	decreased	no
MPH1	YIL002	unchanged	decreased	yes
RFA2-ph	YNL312W	unchanged	decreased	yes
RAD24	YER173W	unchanged	increased	no
RAD59	YDL059C	unchanged	increased	no
SLX8	YER116C	unchanged	increased	no
TOP3	YLR234W	unchanged	increased	no
MRE11	YMR224C	unchanged	unchanged	yes
RAD9	YDR217C	unchanged	increased	yes
RAD50	YGR017W	increased	increased	yes
RAD52	YML032C	increased	increased	yes
XRS2	YDR369C	increased	increased	yes
APJ1	YNL077W	unchanged	unchanged	
ATG29	YPL166W	unchanged	unchanged	
CMR1	YDL156W	unchanged	unchanged	
CSM1	YCR086W	unchanged	unchanged	
CSM3	YMR048W	unchanged	unchanged	
DDC1	YPL194W	unchanged	unchanged	
DUG1	YBR281C	unchanged	unchanged	
DUS3	YLR401C	unchanged	unchanged	
EDC2	YER035W	unchanged	unchanged	
HOS2	YGL194C	unchanged	unchanged	
HPR5/SRS2	YJL092W	unchanged	unchanged	
HTA2	YBL003C	unchanged	unchanged	
LSB1	YGR136W	unchanged	unchanged	
MMS2	YGL087C	unchanged	unchanged	
MMS4	YBR098W	unchanged	unchanged	
MRC1	YCL061C	unchanged	unchanged	
MRT4	YKL009W	unchanged	unchanged	
OAF3	YKR064W	unchanged	unchanged	
PPH21	YDL134C	unchanged	unchanged	
PPH22	YDL188C	unchanged	unchanged	
PPH3	YDR075W	unchanged	unchanged	
PSO2	YMR137C	unchanged	unchanged	
RAD5	YLR032W	unchanged	unchanged	
RAD54	YGL163C	unchanged	unchanged	
RAD55	YDR076W	unchanged	unchanged	
RAD57	YDR004W	unchanged	unchanged	
RFA3-313	YJL173C	unchanged	unchanged	
RMI1	YPL024W	unchanged	unchanged	
RPS18A	YDR450W	unchanged	unchanged	
RTT107	YHR154W	unchanged	unchanged	
SGS1	YMR190C	unchanged	unchanged	
SLX4	YLR135W	unchanged	unchanged	
TEL1	YBL088C	unchanged	unchanged	
TOF1	YNL273W	unchanged	unchanged	
TOF2	YKR010C	unchanged	unchanged	
UBC13	YDR092W	unchanged	unchanged	
YKU70	YMR284W	unchanged	unchanged	
YLR126C	YLR126C	unchanged	unchanged	
YLR363W-A	YLR363W-A	unchanged	unchanged	
YMR111C	YMR111C	unchanged	unchanged	